Biochimica et Biophysica Acta 940 (1988) 105–120
Elsevier

BBA 73978

Changes in both calcium pool size and morphology of human platelets incubated in various concentrations of calcium ion. Calcium-specific bleb formation on platelet-membrane surface

Wei-Jern Tsai [a], Jia-Chyuan Chen [b] and Cheng-Teh Wang [a]

[a] *Institute of Life Science, National Tsing Hua University, Hsingchu,* and [b] *Laboratory of Electron Microscopy, College of Science, National Taiwan University, Taipei (Taiwan, China)*

(Received 23 October 1987)
(Revised manuscript received 3 February 1988)

Key words: Calcium ion flux; Bleb formation; Platelet membrane; Electron microscopy; (Human blood)

In this study, the response of gel-filtered human platelets to extracellular Ca^{2+} at Ca^{2+} concentrations $[Ca^{2+}]_o$ of 1–10 mM was investigated. The distribution of Ca^{2+} among various pools was studied using: (1) quin2, to estimate the cytosolic free Ca^{2+} concentration ($[Ca^{2+}]_i$); and (2) $^{45}CaCl_2$ plus EGTA, to quantitate the sizes of the EGTA-releasable, EGTA-nonreleasable and surface-bound Ca^{2+} pools. The morphological changes were revealed by scanning electron-microscopy (scanning EM), and the effect on thrombin-stimulated aggregation was examined using an aggregometer. Platelets continuously sequestered Ca^{2+} into both EGTA-releasable and EGTA-nonreleasable pools to maintain a low $[Ca^{2+}]_i$ level. The rate of sequestration to the EGTA-releasable pool was independent of $[Ca^{2+}]_o$, while that of the EGTA-nonreleasable pool exhibited first-order kinetics. The cell morphology changed gradually from discoid to the tadpole-like type, and finally to irregular forms. This morphological change correlated with the gradual increase in $[Ca^{2+}]_i$. The EGTA-nonreleasable pool saturated at about 3000 pmol/10^8 cells. This saturation resulted in a drastic increase in the EGTA-releasable pool size, and the cell was lysed concomitantly. The maximum safety capacity of the EGTA-releasable pool was estimated to be 1100 pmol/10^8 cells. The contribution of the cellular compartments to these two pool sizes is extensively discussed. The surface-bound pool size also increased continuously. When two different capacities were reached, i.e., 160 and 600 pmol/10^8 cells, the binding rate increased above the initial rate by 7- and 11-fold, respectively. Hence, the surface-binding capacity might be a critical factor which alters the membrane structure and exposes more binding sites. The cell surface appeared to have blebs, after the binding size had reached more than 600 pmol/10^8 cells. Bleb formation resulted in the inhibition of platelet function. Divalent cations, such as Mg^{2+}, Sr^{2+} and Ba^{2+} did not cause bleb formation, which could mean that this formation is a Ca^{2+}-specific phenomenon.

Introduction

Calcium ion (Ca^{2+}) is important in the regulation of platelet functions [1–3]. Quiescent platelets are able to maintain the cytosolic free Ca^{2+} concentration ($[Ca^{2+}]_i$) at below 0.1 μM [1,4,5]. When platelets are activated, $[Ca^{2+}]_i$ increases to

Abbreviations: EM, electron microscopy; $[Ca^{2+}]_o$, concentration of extracellular Ca^{2+}; $[Ca^{2+}]_i$, concentration of cytosolic free Ca^{2+}; Hepes, 4-(2-hydroxyethyl)-1-piperazineethanesulfonic acid; EGTA, ethylene glycol bis(β-aminoethyl ether)-*N,N,N',N'*-tetraacetic acid; $[M^{2+}]_o$, concentration of extracellular divalent cations; BSA, bovine serum albumin.

Correspondence: C.-T. Wang, Institute of Life Science, National Tsing Hua University, Hsinchu, Taiwan 30043, China.

cause the subsequent physiological responses and morphological changes [1–3,5–7].

The platelet has several compartments in which to store Ca^{2+}. When exposed to a Ca^{2+} solution, the cell is able to maintain a low $[Ca^{2+}]_i$ level [1,4,5]. The Ca^{2+}-specific channel in plasma membrane is responsible for the Ca^{2+} import [8–10]. Plasma membrane exports Ca^{2+} through the Na^+/Ca^{2+} exchanger and an energy-dependent process [11,12]. At physiological external Ca^{2+} concentration ($[Ca^{2+}]_o$), two cellular compartments, i.e., the cytosol and the dense tubular system, are responsible for Ca^{2+} storage [8]. The addition of Ca^{2+}-chelating agent only causes the Ca^{2+}-loaded cells to release a portion of their total Ca^{2+} uptake [8]. The cytosol has an exchangeable pool size of 50 pmol/10^8 cells, irrespective of $[Ca^{2+}]_o$ [8]. The dense tubular system imports Ca^{2+} through a Ca^{2+} pump and releases Ca^{2+} back to cytosol [13–16]. The system accumulates Ca^{2+} in a manner linear to the increase of $[Ca^{2+}]_o$, and this compartment only releases 85% of its loaded Ca^{2+} by ionophore, or 50% by inositol triphosphate [8,15]. In platelets, mitochondria permit relatively little Ca^{2+} accumulation either at 0.8 mM or at 0.1 μM $[Ca^{2+}]_i$, but the compartment takes up and releases Ca^{2+} at higher $[Ca^{2+}]_i$ [8,15]. Dense granule is a Ca^{2+} storage compartment for secretion, its Ca^{2+} uptake from $[Ca^{2+}]_o$ may be very slow [17,18]. In addition, the platelet membrane components, in either the plasma membrane or the cytoplasmic surface of organelles, operate Ca^{2+} sequestration and release [16]. A recent study has estimated the binding affinity of membrane phospholipids to Ca^{2+} [19]. In addition, the platelet surface can bind external Ca^{2+} with 57000 and 460000 binding sites per cell for the high- and the low-affinity binding, respectively [20]. Therefore, during storage of platelets in high $[Ca^{2+}]_o$ level, all of the cellular compartments may take charge of the Ca^{2+} storage.

Platelets activated by agonist undergo shape change and secretion [1–3]. This morphological change is due to the elevation of $[Ca^{2+}]_i$, because the change results from the sensitivity of cytoskeletal molecules to $[Ca^{2+}]_i$ in the nanomolar range. The phenomena include: (1) polymerization of actin monomers; (2) reorganization of actin filaments; (3) dissociation of microtubules; and (4) repolymerization of microtubules [21–28]. During storage of platelets in high $[Ca^{2+}]_o$, if $[Ca^{2+}]_i$ in the cell appears to increase gradually, the cell morphology may change.

It is well known that high $[Ca^{2+}]_o$ is toxic to cells. Murer [29] had reported that high $[Ca^{2+}]_o$ inhibits the platelet function. However, the tolerance of platelets to high $[Ca^{2+}]_o$ remains to be investigated. To this end, in this study, we investigated how human platelets responded to storage in various levels of $[Ca^{2+}]_o$. Three investigations were performed. The Ca^{2+} flux study estimated the distribution of Ca^{2+} among various cellular pools. Scanning electron microscopy revealed the morphological change, and the thrombin-stimulated aggregation indicated the Ca^{2+} effect on platelet function. The results show that platelets continuously sequester Ca^{2+} from the external environment and deform gradually. The cell-surface Ca^{2+}-binding property alters gradually during storage, and the Ca^{2+}-specific bleb might appear on the surface causing the inhibition of platelet function. Preliminary reports of this work have appeared elsewhere [30–32].

Experimental Procedure

Materials

Chemicals and organic solvents were purchased from E. Merck (Darmstadt, F.R.G.). All organic solvents were redistilled before use. The following reagents were obtained from Sigma (St. Louis, MO, U.S.A.): apyrase, indomethacin, quin2 acetoyoxymethyl ester (quin2/AM), bovine thrombin, NADH, lactate dehydrogenase (from porcine muscle type XXIX), fatty acid-free bovine serum albumin (BSA). Sepharose 2B was from Pharmacia Fine Chemicals (Piscataway, NJ, U.S.A.). The $^{45}CaCl_2$ (22 Ci/g Ca^{2+}) was obtained from ICN (Irvine, CA, U.S.A.). The carrier-free [^{32}P]phosphate (2 mCi/ml, pH 7.4) was a generous gift from the Department of Radioiostope, National Tsing Hua University, Hsinchu, Taiwan, China.

Methods

Preparation of gel-filtered platelets suspension. Human venous blood was drawn from healthy adult donors, who said they had taken no drugs

for at least 2 weeks, and was anticoagulated with one ninth volume of 0.11 M sodium citrate. The citrated blood was centrifuged by swinging centrifugation at $250 \times g$ for 15 min at room temperature. The platelet-rich plasma was applied onto a Sepharose 2B column to isolate gel-filtered platelets [32]. The isolation medium consisted of modified Ca^{2+}-free Tyrode's buffer containing 137 mM NaCl, 2.7 mM KCl, 1 mM $MgCl_2$, 0.4 mM NaH_2PO_4, 2.8 mM glucose, 12 mM $NaHCO_3$ and 0.2% BSA (pH 7.4). Cell number was counted by a hemocytometer from a phase-contrast microscope (Nikon, Type 104, Tokyo, Japan).

Estimation of Ca^{2+}-pool sizes in platelets. Commercially available quin2/AM was employed to measure $[Ca^{2+}]_i$ of platelets during storage at various $[Ca^{2+}]_o$ levels. The assay was performed in the same way as that described by Tsien et al. [33]. Gel-filtered platelets ($3 \cdot 10^8$ cells/ml) were incubated with 15 μM quin2/AM in dimethylsulfoxide at 37 °C for 30 min. The suspension was then centrifuged to remove any extraneous dye at $1000 \times g$ for 20 min at room temperature. The pellet was resuspended with the same volume of Ca^{2+}-free Hepes/Tyrode's buffer (pH 7.4), in which BSA had been substituted by 5 mM Hepes. The suspension was warmed up to 37 °C for 30 min before addition of Ca^{2+} at various $[Ca^{2+}]_o$. At a specific incubation stage, an aliquot was transferred into a siliconized quartz cuvette prewarmed at 37 °C in the fluorescence spectrophotometer (Hitachi, Model 650-60, Japan). The fluorescence was measured at an excitation wavelength of 339 nm and an emission wavelength of 490 nm. The $[Ca^{2+}]_i$ was calibrated according to the method described by Tsien et al. [33]. The control experiment showed that quin2 did not leak from the quin2-loaded platelets which were preincubated in $[Ca^{2+}]_o \leq 5$ mM for 3 h. The experiments were performed by centrifuging the mixture. The supernatant appeared to have no detectable fluorescence at 490 nm.

$^{45}CaCl_2$ and EGTA were employed to identify the Ca^{2+}-pool sizes in platelets as the EGTA-releasable, EGTA-nonreleasable and surface-bound pools. The experiment was performed similarly to that described by Brass [20]. In general, gel-filtered platelets ($3 \cdot 10^8$ cells/ml) after preincubation at 37 °C for 30 min, were incubated with various concentrations of Ca^{2+} ($[Ca^{2+}]_o$) containing $^{45}CaCl_2$ (5 μCi/ml). At a specific stage, an aliquot was transferred to the top of a silicon oil layer in an Eppendorf tube and centrifuged at $12000 \times g$ for 2 min by Eppendorf centrifuge (Eppendorf, Model 5414, Hamburg, F.R.G.). The supernatant was decanted and the pellet was wiped dried with a Q-tip. The pellet was then transferred into a counting vial with 5 ml of Econofluor (New England Nuclear), and the radioactivity was measured to calibrate the Ca^{2+} content by a liquid scintillation counter (Beckman, LS100C, Irvine, CA, U.S.A.).

Specifically, the following procedures were performed to calibrate each Ca^{2+}-pool size. The incubation mixture was divided into three equal parts. The first aliquot was directly centrifuged through a silicon oil layer. The radioactivity in the pellet was a measure for the total platelet Ca^{2+} loading (I), which represented the Ca^{2+} load in the EGTA-releasable, EGTA-nonreleasable and surface-bound pools. The second aliquot was added with 20 mM EGTA immediately prior to centrifugation to obtain the cellular Ca^{2+} total uptake (II). By this transient chelation, EGTA might remove almost all of surface-bound Ca^{2+}. Hence, the difference between (I) and (II) equalled the surface-bound Ca^{2+} pool size. To obtain the EGTA-nonreleasable pool size (III), the third aliquot was incubated with 20 mM EGTA for 60 min before centrifugation. No significant difference in radioactivity was found from the pellets obtained by centrifuging the aliquots which had been incubated with EGTA for 60 and 90 min. Hence, the EGTA-releasable pool size was calculated from the difference between (II) and (III). The EGTA-releasable pool represented only the amount of the cellular Ca^{2+} which could be chelated by external EGTA.

Morphological study by scanning electron microscopy. The sample preparation was described previously [32]. In brief, gel-filtered platelets were first added either with apyrase (200 μg/ml) plus 10 μM indomethacin or without and were then incubated with various $[Ca^{2+}]_o$ at 37 °C. After a given period, aliquots were fixed at 4 °C for 30 min by adding 5 volumes of ice-cold modified Ca^{2+}-free Tyrode's buffer containing 2.5% glutaraldehyde. The suspension was then centri-

fuged at 1000 × g for 20 min at 4°C. The pellet was washed with cold buffer three times and post-fixed with cold buffer containing 1% osmium tetroxide for 1 h. The sample was rinsed with buffer and dehydrated in a graded series of ethyl alcohol concentrations. After another two rinses with 100% acetone, the sample was dried in a CO_2 critical point dryer (Hitachi, HCP-2, Japan). The dried sample was coated with gold in Ion Coater (Eiko Engineering, Model IB-2). The cell morphology was revealed under an Hitachi S-520 scanning electron microscope at 20 kV.

Other studies. An aggrecoder (Hitachi, Model PA-3210, Japan) was used to study platelet function [32]. To determine the leakiness of the plasma membrane, analysis of lactate dehydrogenase activity was performed according to the method of Bergmeyer et al. [34]. The release of serotonin, a characteristic of dense granule release, was assayed according to the procedure described by Drummond et al. [35]. To determine whether autohydrolysis of platelet phospholipids appeared, the change in [^{32}P]phospholipids of [^{32}P]phosphate-labeled platelets was investigated as described previously [32].

Results

The Ca^{2+}-uptake of human platelets incubated with various concentrations of extracellular Ca^{2+}

Figs. 1–4 show the time courses of the increase in $[Ca^{2+}]_i$ and those of Ca^{2+} uptake into the EGTA-releasable, EGTA-nonreleasable and surface-bound pools. Platelets sequestered a mass of Ca^{2+} into each pool during the first minute of incubation. Then a slower rate appeared. The sizes of the Ca^{2+} pools at 1 min, 90 min and 3 h of incubations are shown in Table I.

Platelets maintained $[Ca^{2+}]_i$ at a low level even after prolonged incubation in various $[Ca^{2+}]_o$ (Fig. 1). The rate of $[Ca^{2+}]_i$ elevation was concentration dependent. In $[Ca^{2+}]_o \leq 5$ mM, the time-course profile was biphasic. Initially, the V_{max} was 2.3 nM/min as estimated from a double-reciprocal plot (data not shown). When $[Ca^{2+}]_i$ reached 140 nM, the rate was doubled (V_{max} = 3.8 nM/min). In $[Ca^{2+}]_o \leq 7.5$ mM, the time course showed a linear increase in $[Ca^{2+}]_i$ with a rate of 3

TABLE I

THE Ca^{2+}-POOL SIZES OF HUMAN PLATELETS INCUBATED WITH VARIOUS CONCENTRATIONS OF EXTRACELLULAR Ca^{2+}

Details of the experimental procedure and the calibrations of pool size are described in Materials and Methods. The EGTA-releasable and EGTA-nonreleasable pools, each of which involve several compartments, as well as the surface-bound pool are shown in Fig. 10. These compartments are the membrane system which includes the plasma membrane and the cytoplasmic surface of organelle membrane, cytosolic molecules, dense tubular system and mitochondria. At different $[Ca^{2+}]_o$, these compartments may contribute different amounts to both the EGTA-releasable and the EGTA-nonreleasable pool sizes. The surface-bound pool represents only the bound Ca^{2+} readily releasable by a transient EGTA chelation. Data (mean ± S.D.) were taken from at least ten independent experiments.

Ca^{2+} pool	$[Ca^{2+}]_o$ (mM)	Ca^{2+}-pool size at the time of incubation (pmol/10^8 cells)		
		1 min	90 min	180 min
EGTA-releasable	1	13 ± 4	250 ± 21	350 ± 30
	5	199 ± 12	733 ± 67	1100 ± 133
	10	495 ± 50	1190 ± 96	2677 ± 233
EGTA-nonreleasable	1	82 ± 10	613 ± 50	900 ± 95
	5	506 ± 23	1550 ± 89	1988 ± 159
	10	1485 ± 75	3083 ± 167	3516 ± 210
Surface-bound	1	50 ± 6	130 ± 11	567 ± 36
	5	95 ± 10	10044 ± 432	23172 ± 1596
	10	603 ± 36	44130 ± 1073	89883 ± 2375

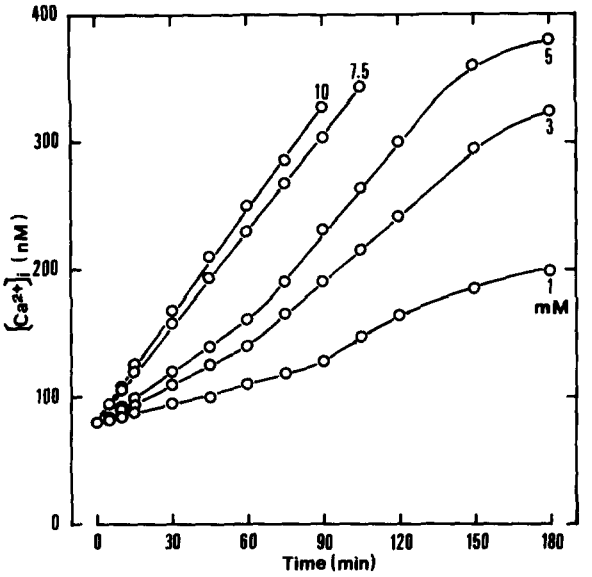

Fig. 1. The elevation of $[Ca^{2+}]_i$ in gel-filtered platelets incubated in various $[Ca^{2+}]_o$. Quin2-loaded platelets ($3 \cdot 10^8$ cells/ml) were warmed to 37 °C for 30 min, then incubated with various $[Ca^{2+}]_o$. The values of $[Ca^{2+}]_o$, in mM, are indicated in the figure. At a given stage of incubation, the cell suspension was transferred into a siliconized cuvette (prewarmed at 37 °C) for measuring the fluorescence change in a fluorescence spectrophotometer. Data points were the mean values of eight experiments.

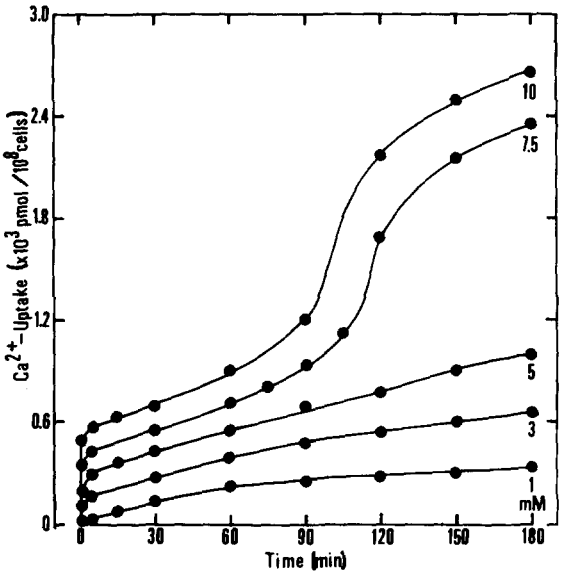

Fig. 2. Time course of Ca^{2+} uptake into the EGTA-releasable pool of gle-filtered platelets incubated in various $[Ca^{2+}]_o$. Gel-filtered platelets ($3 \cdot 10^8$ cells/ml), preincubated at 37 °C for 30 min, were added with $CaCl_2$ to a final $[Ca^{2+}]_o$ (in mM) as indicate in the figure. $^{45}CaCl_2$ (5 μCi/ml) was added as probe. Calibration of Ca^{2+} uptake and details of the experimental procedures are described in Materials and Methods. Data points are the mean values of at least ten experiments.

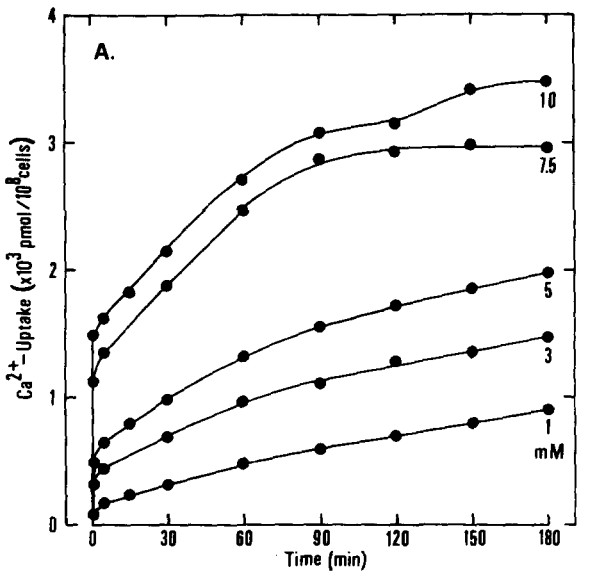

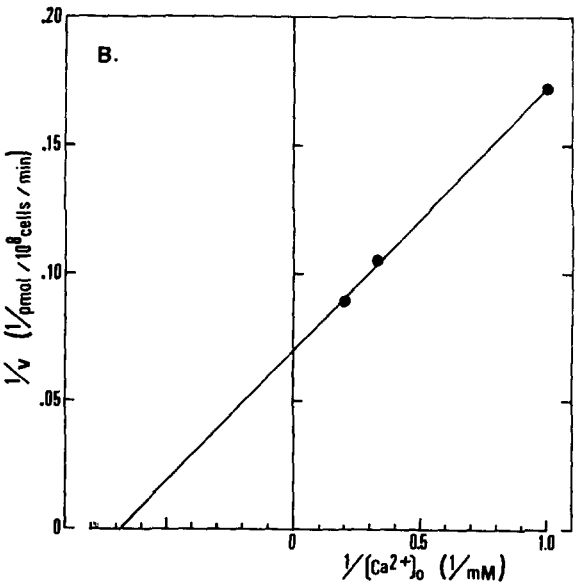

Fig. 3. (A) Time course of Ca^{2+} uptake into the EGTA-nonreleasable pool of gel-filtered platelets incubated in various $[Ca^{2+}]_o$. The values of $[Ca^{2+}]_o$ (in mM) are indicated in the figure. Details of the experimental procedures and calibration of the Ca^{2+} uptake are described in Fig. 2 and in Materials and Methods. Data points are the mean values of at least ten experiments. (B) A double-reciprocal plot of $[Ca^{2+}]_o$ vs. the rate of Ca^{2+} uptake into the EGTA-nonreleasable pool. The rate of uptake was determined from 5 min to 60 min of incubation of the platelets in $[Ca^{2+}]_o \leq 5$ mM. ($V_{max} = 14.1$ pmol/10^8 cells per min; $K_m = 1.43$ mM).

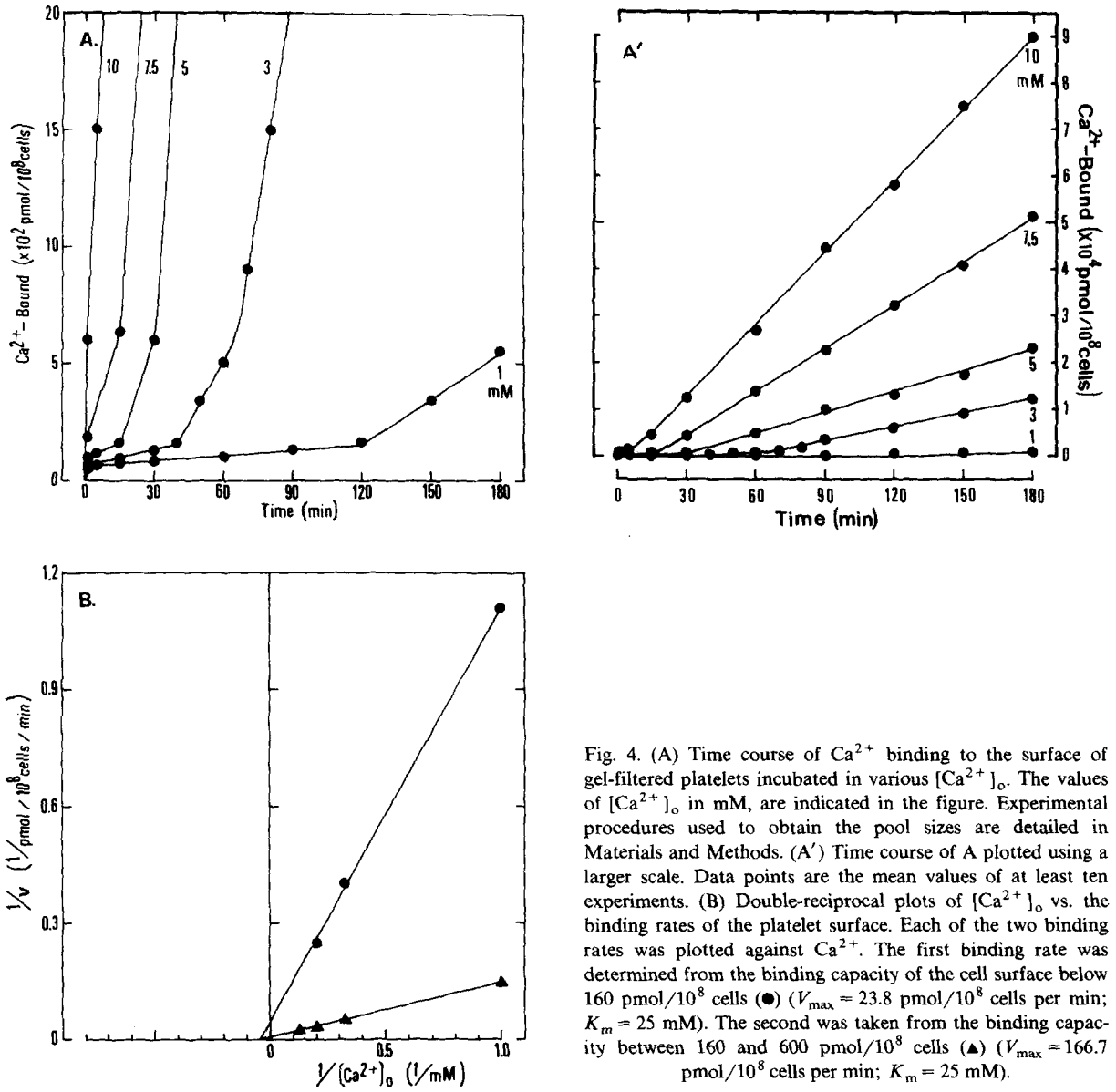

Fig. 4. (A) Time course of Ca^{2+} binding to the surface of gel-filtered platelets incubated in various $[Ca^{2+}]_o$. The values of $[Ca^{2+}]_o$ in mM, are indicated in the figure. Experimental procedures used to obtain the pool sizes are detailed in Materials and Methods. (A') Time course of A plotted using a larger scale. Data points are the mean values of at least ten experiments. (B) Double-reciprocal plots of $[Ca^{2+}]_o$ vs. the binding rates of the platelet surface. Each of the two binding rates was plotted against Ca^{2+}. The first binding rate was determined from the binding capacity of the cell surface below 160 pmol/10^8 cells (●) (V_{max} = 23.8 pmol/10^8 cells per min; K_m = 25 mM). The second was taken from the binding capacity between 160 and 600 pmol/10^8 cells (▲) (V_{max} = 166.7 pmol/10^8 cells per min; K_m = 25 mM).

nM/min (Fig. 1). The cells became leaky at this high $[Ca^{2+}]_o$ for over 90 min, as indicated by the leakiness of lactate dehydrogenase (data not shown). Therefore, $[Ca^{2+}]_i$ determined under these conditions might be invalid. In addition, the incubated platelets did not show: (1) the release of serotonin; (2) the leakiness of lactate dehydrogenase; and (3) the change in radioactivity of [^{32}P]phospholipids studied from [^{32}P]phosphate-labelled platelets (data not shown). This indicates

Fig. 5. Scanning electron micrograph of gel-filtered platelets incubated in 1 mM $[Ca^{2+}]_o$ (original magnification ×9000, reproduction (7/8)). Gel-filtered platelets obtained at room temperature (A) were incubated in Ca^{2+}-free medium at 37 °C for 30 min (B). The prewarmed platelets were then incubated with 1 mM $[Ca^{2+}]_o$ for 1 min (C), 5 min (D), 30 min (E), 90 min (F), 120 min (G) and 150 min (H). T and I in G and H indicate the tadpole-like cell and the irregular form, respectively. Details of the experiments are given in Materials and Methods.

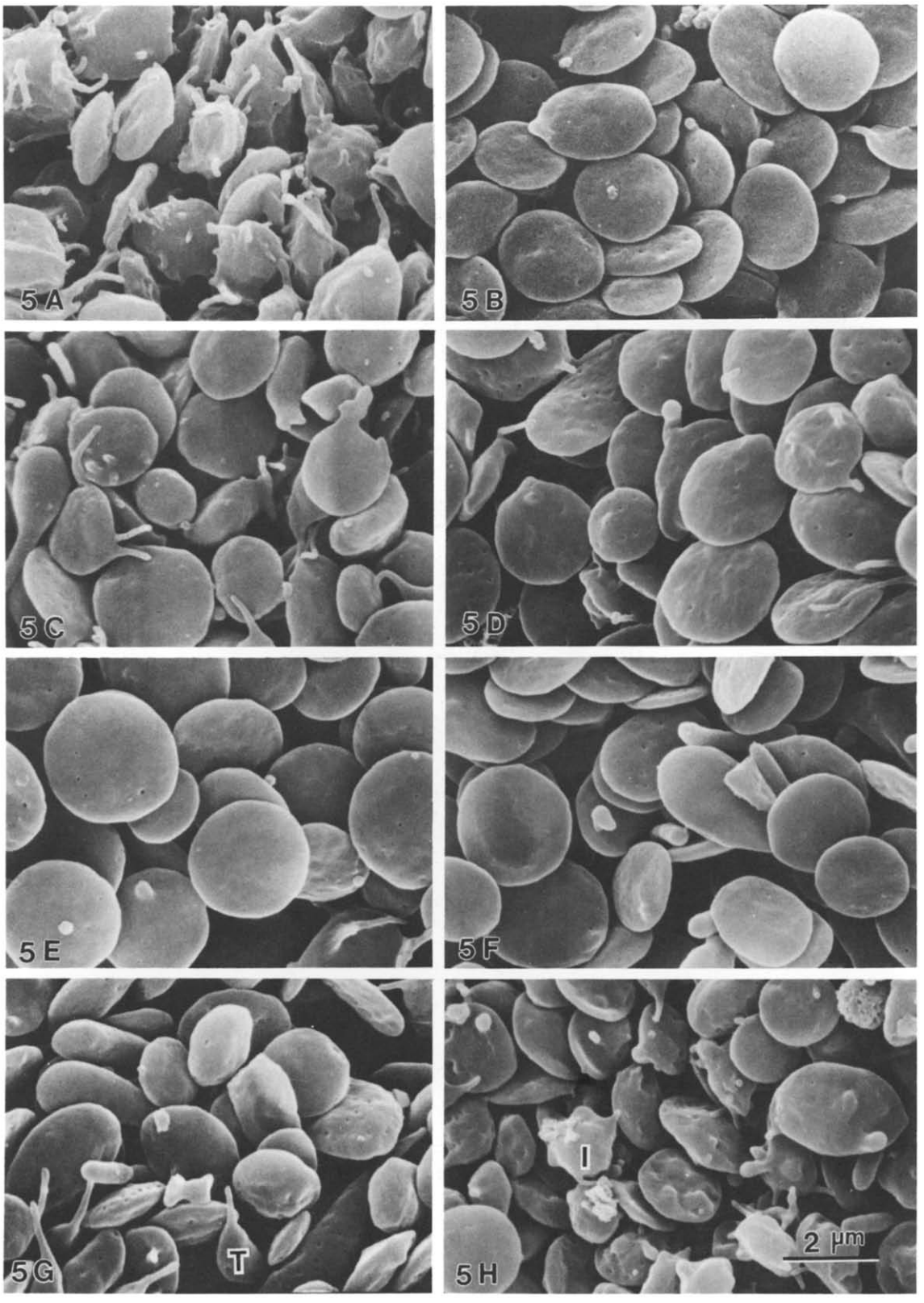
5 A
5 B
5 C
5 D
5 E
5 F
5 G
T
5 H
I
2 µm

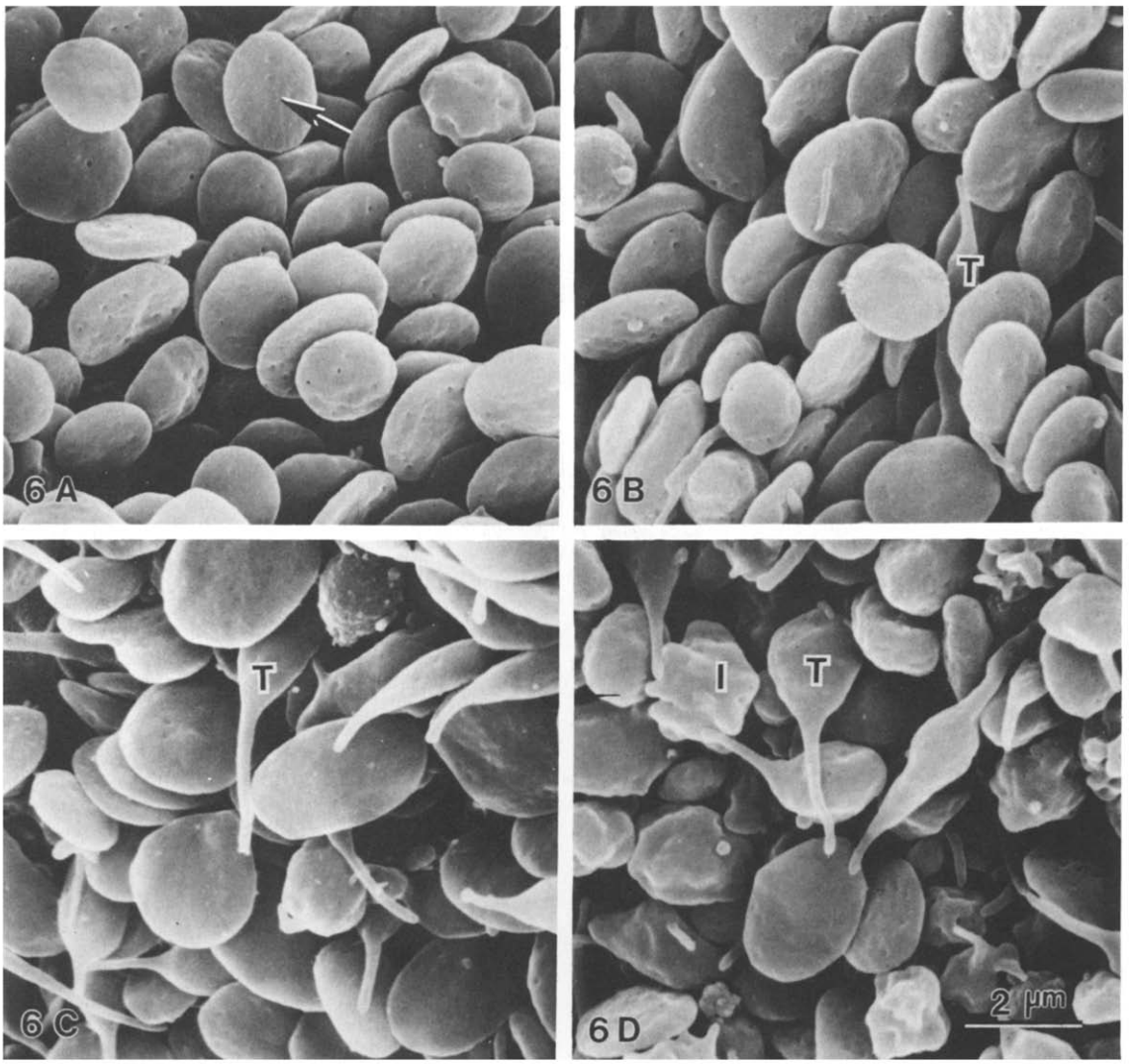

Fig. 6. Scanning electron micrographs of gel-filtered platelets incubated in 5 mM $[Ca^{2+}]_o$ (original magnification×9000, reproduction (7/8)). Gel-filtered platelets were preincubated at 37° C for 30 min, and were then added to 5 mM $[Ca^{2+}]_o$ for 30 min (A), 60 min (B), 90 min (C) and 150 min (D). Arrows (←), and T and I indicate the blebs on the cell surface, the tadpole-like cells and irregular forms, respectively. Details of the experiments are given in Materials and Methods.

that the gradual $[Ca^{2+}]_i$ increase in platelets resulted in neither secretion nor phospholipase activation.

During the first minute of incubation, the size of both EGTA-releasable and EGTA-nonreleasable pools increased with first-order kinetics (Figs. 2 and 3 and Table I). Then, the rates for accumulating these two pools appeared to be different.

Fig. 7. Scanning electron micrographs of gel-filtered platelets incubated in 10 mM $[Ca^{2+}]_o$ (original magnification×9000, reproduction (7/8)). Gel-filtered platelets were prewarmed at 37° C for 30 min, and then were incubated with 10 mM $[Ca^{2+}]_o$ for 5 min (A), 15 min (B), 30 min (C), 90 min (D) and 120 min (E). In addition, the platelets, after 30 min ageing in 10 mM $[Ca^{2+}]_o$, were added with 20 mM eGTA and then fixed immediately (F). Arrows (←) indicate the blebs on the platelet surface. T, I and S indicate the tadpole-like cells, the irregular form and the spongy-like cells, respectively. Details of the experiments are given in Materials and Methods.

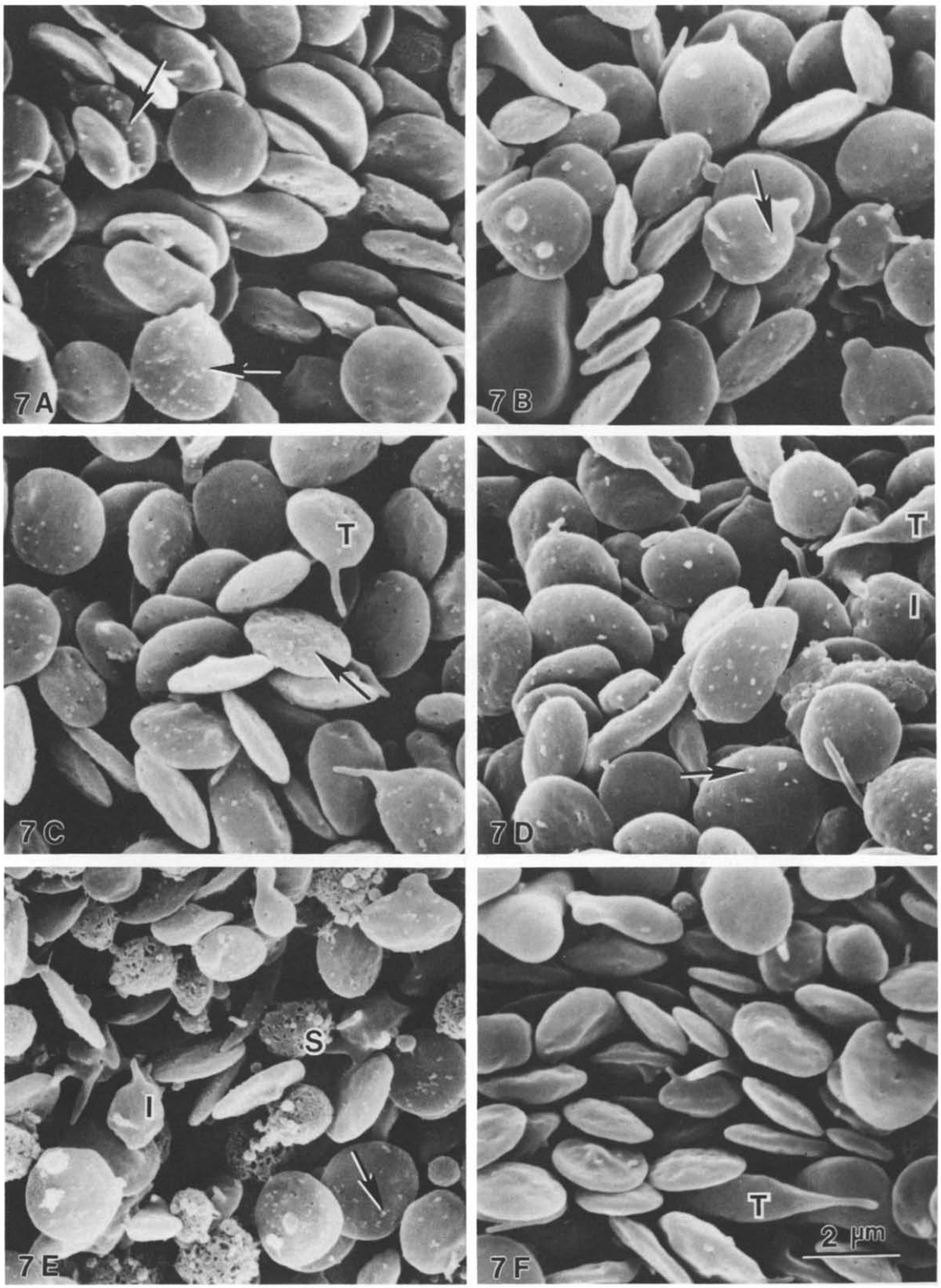
7A
7B
T
7C
T
I
7D
S
I
7E
T
2 µm
7F

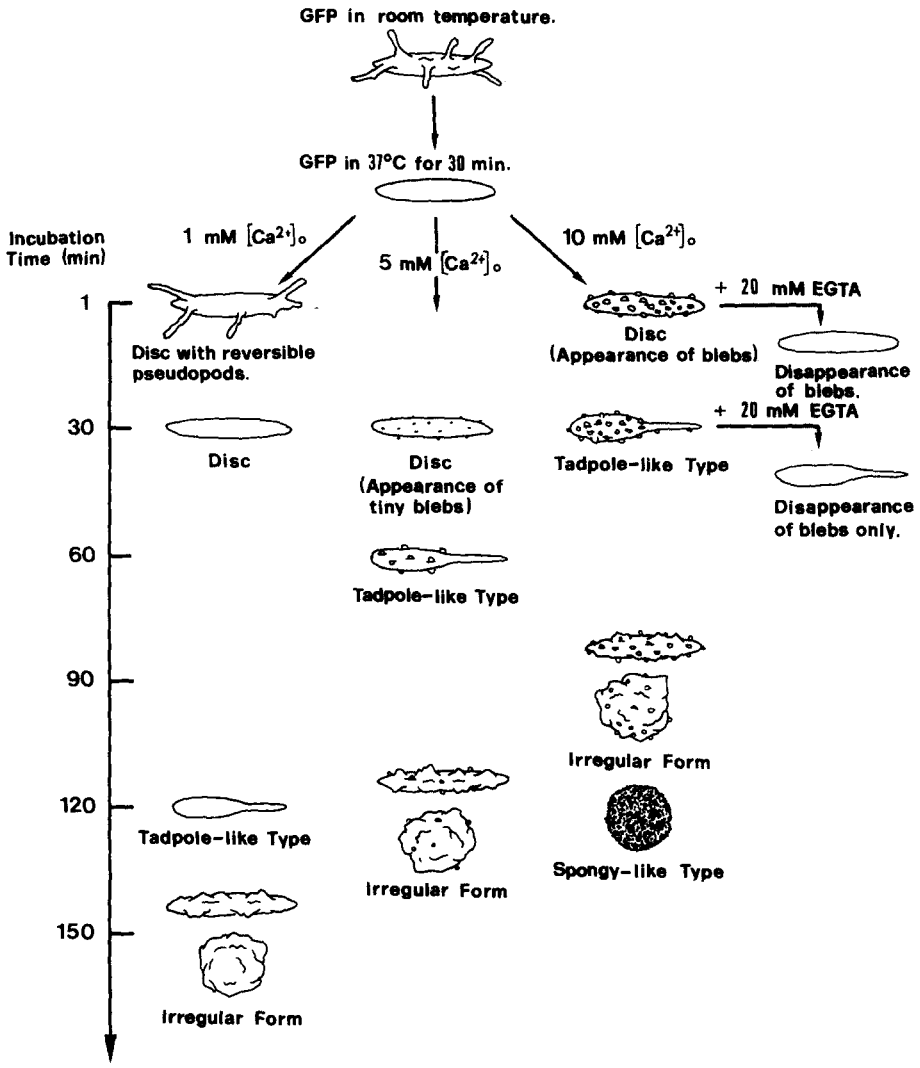

Fig. 8. Schematic representation of the sequential morphological changes of gel-filtered platelets incubated in various $[Ca^{2+}]_o$.

The rate for the EGTA-releasable pool was concentration independent with 4.0–4.7 pmol/10^8 cells per min (Fig. 2). A drastic increase in the EGTA-releasable pool appeared after the cells were incubated either in 7.5 mM $[Ca^{2+}]_o$ for 105 min or in 10 mM $[Ca^{2+}]_o$ for 90 min (Fig. 2). In both cases, a similar pool size, found to be 1100 pmol/10^8 cells, was observed. The size might represent a safety capacity for this pool.

The rate of the EGTA-nonreleasable pool was with first-order kinetics at $[Ca^{2+}]_o \leq 5$ mM (Fig. 3A). Fig. 3B is a double-reciprocal plot of $[Ca^{2+}]_o$ vs. the rate which was estimated from 5 min to 60 min incubation. The V_{max} and K_m were 14.1 pmol/10^8 cells per min and 1.43 mM, respectively. Then, the rate started to decline to a steady

Fig. 9. Scanning electron micrographs of gel-filtered platelets incubated in various $[M^{2+}]_o$ (original magnification ×9000, reproduction (7/8)). Gel-filtered platelets isolated in Ca^{2+}-free media were prewarmed at 37 °C for 30 min. The platelets were then incubated with 5 mM $[Mg^{2+}]_o$ (A), $[Sr^{2+}]_o$ (C) or $[Ba^{2+}]_o$ (E) for 60 min, and with 10 mM $[Mg^{2+}]_o$ (B), $[Sr^{2+}]_o$ (D) or $[Ba^{2+}]_o$ (F) for 5 min. Details of the experiments are given in Materials and Methods.

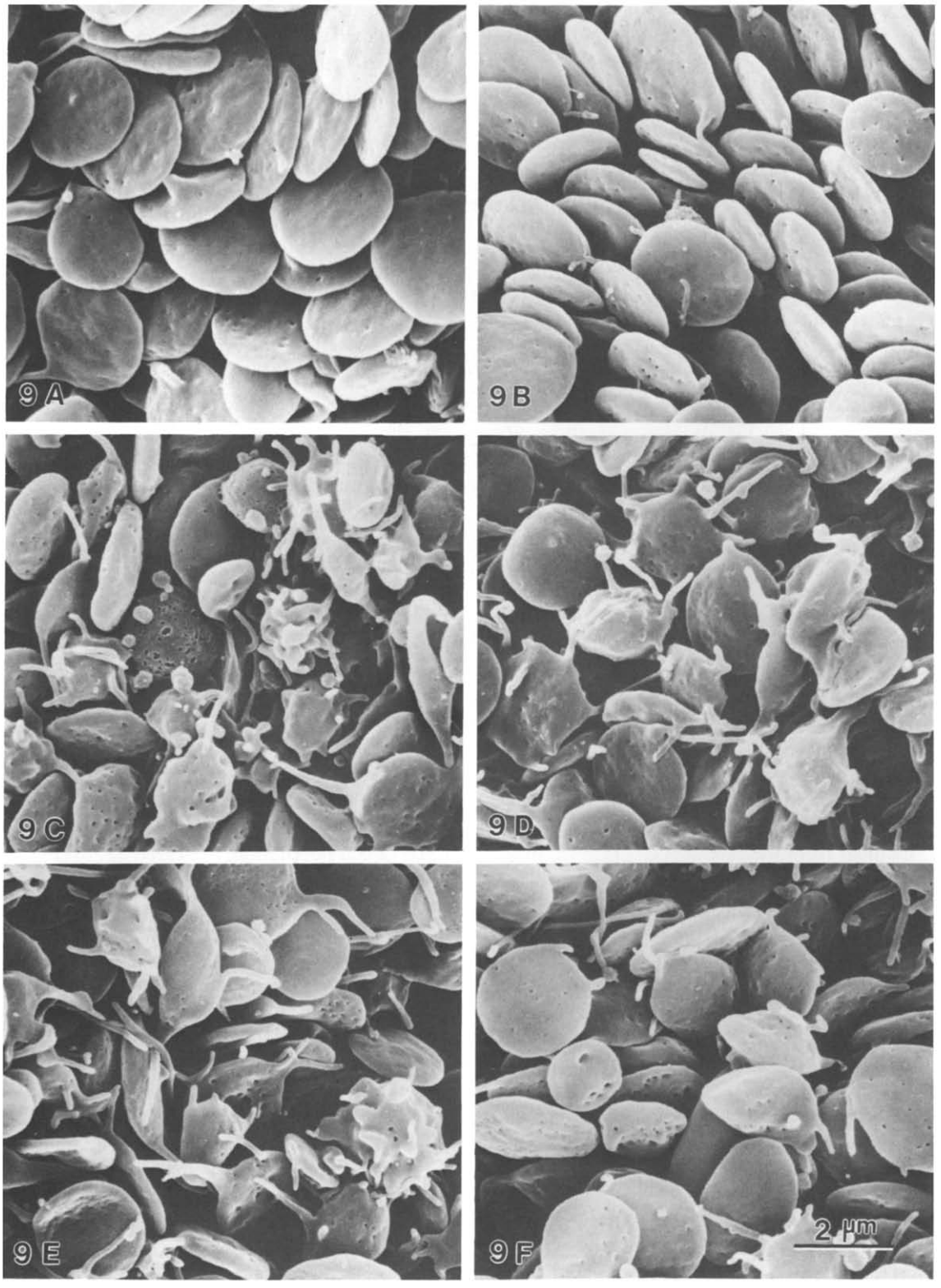
9A
9B
9C
9D
9E
9F
2 µm

state at either 1 mM $[Ca^{2+}]_o$ for 90 min or 5 mM $[Ca^{2+}]_o$ for 60 min (Fig. 3A). Interestingly, these two situations also showed the rate change of the increase in $[Ca^{2+}]_i$ (Fig. 1). Hence, the correlation may imply that the increase in $[Ca^{2+}]_i$ was due to the rate declination of the EGTA-nonreleasable pool to a steady state. Another correlation found was that of the saturation of EGTA-nonreleasable pool causing a drastic size increase in the EGTA-releasable pool. This was the case for platelets incubated either in 7.5 mM $[Ca^{2+}]_o$ for 105 min or in 10 mM $[Ca^{2+}]_o$ for 90 min (Figs. 2 and 3 and Table I). Therefore, the EGTA-nonreleasable pool might become saturated at about 3000 pmol/10^8 cells.

The surface Ca^{2+}-binding rate was also concentration dependent (Fig. 4). However, three different binding rates appeared (Fig. 4A). The binding rate altered twice after the surface binding capacity had reached two different capacities, i.e., 160 and 600 pmol/10^8 cells. The first alteration was found in platelets incubated in 1, 3 or 5 mM $[Ca^{2+}]_o$ for 120, 40 and 15 min, respectively (Fig. 4A). Under these conditions, the binding capacity for all was about 160 pmol/10^8 cells (equivalent to $9.6 \cdot 10^8$ sites/cell). The second alteration was observed in platelets incubated in 3 and 5 mM $[Ca^{2+}]_o$ for 65 and 30 min, respectively (Fig. 4A). The capacity was about 600 pmol/10^8 cells ($3.7 \cdot 10^8$ sites/cell). After the second alteration, a faster, third binding rate appeared with first-order kinetics. The V_{max} was 255 pmol/10^8 cells per min, obtained from the rate at $[Ca^{2+}]_o \geq 7.5$ mM. Fig. 4B shows two double-reciprocal plots of $[Ca^{2+}]_o$vs. two kinds of binding rate. The first one was obtained from the initial rate (before the first alteration), and the second one was taken from the rates between the two alterations. The plots indicate that: (1) initially, the cell-surface-bound Ca^{2+} had a V_{max} of 23.8 pmol/10^8 cells per min; and (2) the V_{max} changed to 166.7 pmol/10^8 cells per min after the first alteration. When the cells were incubated in 10 mM $[Ca^{2+}]_o$ for only 1 min, the surface-bound Ca^{2+} was above 600 pmol/10^8 cells (Table I). Hence, only the third Ca^{2+}-binding rate appeared (Fig. 4A).

In summary, the results show that platelets continuously sequestered Ca^{2+} from the external medium into the EGTA-releasable pool with V_{max}, and into the EGTA-nonreleasable pool with first-order kinetics. Also, incubation of platelets resulted in the alteration of the cell-surface Ca^{2+}-binding property.

Scanning electron micrographs of platelets incubated in various extracellular Ca^{2+} concentrations

Platelets continuously sequestered Ca^{2+} into each pool during prolonged incubation in various $[Ca^{2+}]_o$. It is possible that the cell morphology may change. Scanning EM was employed to examine the possible morphological change at each incubation stage (Figs. 5–7). The morphological change appeared to be similar in cells treated with either apyrase plus indomethacin or without. Hence, the result might mean a direct Ca^{2+} effect on the cell morphology. Fig. 8 is a schematic drawing summarizing the morphological change of platelets incubated in various $[Ca^{2+}]_o$.

Isolated gel-filtered platelets deformed at room temperature (Fig. 5A) and resumed their discoid shape after incubation at 37°C for 30 min (Fig. 5B). On addition of 1 mM $[Ca^{2+}]_o$ into this prewarmed cell suspension, the cells immediately deformed into puffy discs with the pseudopod protrusion as found after 1 min of incubation (Fig. 5C). However, platelets were able to regulate this kind of Ca^{2+} stress. The cell resumed its discoid shape without pseudopod at 5 min (Fig. 5D), then the disoid-shaped cell flattened out by 30 min (Fig. 5E). Platelets remained as discs at 90 min (Fig. 5F), subsequently the tadpole-like cells (35% of cell population) appeared at 2 h (Fig. 5G). At 150 min, 30% of cells deformed into the irregular forms (Fig. 5H).

On increasing $[Ca^{2+}]_o$ to 5 mM, an interesting morphological feature appeared. At 30 min, the tiny blebs showed up on the surface of the flattened discs (Fig. 6A). This cell type increased in number after prolonged incubation. At 60 min, about 30% of platelets changed to the tadpole-like type (Fig. 6B). This type of cell increased to 50% of the population at 90 min (Fig. 6C). At 150 min, platelets became irregular in form (Fig. 6D).

When platelets were incubated in 10 mM Ca^{2+}, blebs appeared on the cell surface after 1 min and remained on the surface after a prolonged period of incubation (Fig. 7A–E). The bleb size was larger than that found on the cell incubated in 5

mM $[Ca^{2+}]_o$, and the bleb number on each cell was also more than that appearing on the cells stored in 5 mM $[Ca^{2+}]_o$ (Fig. 6). Tadpole-like cells appeared at 30 min (about 10% of cell population) (Fig. 7C). The cells deformed into the irregular forms, and some lysed cells appeared as a spongy-like sphere at 90 min (Fig. 7D). The lysed cells comprised 40% of the population at 120 min (Fig. 7E). Comparison between the morphological change and the Ca^{2+} flux studies (Figs. 2 and 3) showed that the cell lysis might correlate with the drastic increase in the EGTA-releasable pool, which resulted from the saturation of the EGTA-nonreleasable pool. Another interesting finding was that addition of 20 mM EGTA abolished the cell-surface blebs, but not the pseudopods (Fig. 7F). Hence, excess surface bound Ca^{2+} might cause the bleb formation on the cell surface, while the pseudopod might be due to the Ca^{2+} effect from the intracellular compartments, such as the slow increase in $[Ca^{2+}]_i$.

Effect of Mg^{2+}, Sr^{2+} and Ba^{2+} on platelet morphology and function

Divalent cations, such as Mg^{2+}, Sr^{2+} and Ba^{2+} were employed for comparison with the Ca^{2+} effect on platelet morphology (Fig. 9). The intention was to answer the question of whether bleb formation is a Ca^{2+}-specific phenomenon. The cells were incubated in 5 and 10 mM $[M^{2+}]_o$ for 60 and 5 min, respectively. Under these two sets of conditions, Ca^{2+} could induce bleb formation (Figs. 6B and 7A). The scanning EM study revealed that: (1) the Mg^{2+}-treated platelets remained discoid in shape (Figs. 9A–B); (2) platelets treated with either Sr^{2+} or Ba^{2+} deformed into irregular forms with pseudopod protrusion (Figs. 9C–F); and (3) no bleb was found in all of these preparations (Fig. 9). Hence, bleb formation might be a Ca^{2+}-specific phenomenon (Fig. 7).

The effects of these ions on thrombin-stimulated platelet aggregation were also compared with the effect of Ca^{2+} (Table II). In comparison with the control experiment, the Ca^{2+} (10 mM $[Ca^{2+}]_o$) affected the cells by (1) prolonging the period of shape change by 2-fold; (2) inhibiting 45% of the initial aggregation rate; and (3) reducing 15% of platelet aggregation. Although Mg^{2+} exhibited an effect similar to that of Ca^{2+} in prolonging the period of shape change and inhibiting the initial aggregation rate, it inhibited platelet aggregation more than Ca^{2+} did. On the other hand, Sr^{2+} and Ba^{2+} did not cause any significant inhibition of the period of shape change and the initial aggregation rate, but these two ions inhibited 35% of cell aggregation. Hence, the effects of these three ions on platelet function were also different from that of Ca^{2+}. In addition, the EGTA-washed cells which were preincubated in 10 mM $[Ca^{2+}]_o$ for 5 min responded in a manner similar to that of the control. Hence, bleb formation might be the primary cause of the inhibition of platelet function by Ca^{2+}. Currently, studies are being carried out in this laboratory on the effect of high $[Ca^{2+}]_o$ on biochemical events in platelets.

TABLE II

EFFECTS OF DIVALENT CATIONS ON THE THROMBIN-STIMULATED PLATELET AGGREGATION

The platelet function was recorded on an aggrecorder. Gel-filtered platelet suspensions ($1.5 \cdot 10^8$ cells/0.5 ml) were incubated in various $[M^{2+}]_o$ at 37 °C for 5 min, and then 0.05 units of bovine thrombin was added. The shape change period represents the time between the addition of thrombin and the minimum transmission observed on an aggrecorder. The initial aggregation rate was obtained from the initial slope of the aggregation curve represented as percentage of platelet aggregation per minute.

$[M^{2+}]_o$	Shape change period (s)	Initial aggregation rate (%/min)	% of aggregation
Control	10±1	75±10	100± 5
10 mM $[Ca^{2+}]_o$	25±5	40± 8	85±10
10 mM $[Mg^{2+}]_o$	20±6	50± 5	70±12
10 mM $[Sr^{2+}]_o$	12±3	70± 4	65±10
10 mM $[Ba^{2+}]_o$	12±2	69± 5	67±11
5 mM $[Ca^{2+}]_o$	12±3	68±10	92± 5
1 mM $[Ca^{2+}]_o$	10±2	72± 9	98± 4
10 mM $[Ca^{2+}]_o$ and EGTA washed	10±2	77± 6	100± 3

Discussion

This study demonstrates that human platelets, incubated in high $[Ca^{2+}]_o$, continuously take Ca^{2+} up into the cellular compartments and bind Ca^{2+} on the cell surface (Figs. 1–4). During storage in $[Ca^{2+}]_o$, the cell appears to have a low rate of

$[Ca^{2+}]_i$ increase (Fig. 1) and, hence, maintains a low $[Ca^{2+}]_i$ level. This continuous increase in $[Ca^{2+}]_i$ may correlate with the gradual change in morphology as revealed by scanning EM (Figs. 5–7). Incubation of the cells in high $[Ca^{2+}]_o$ may not only cause the saturation of the cellular Ca^{2+}-storage compartments, but also modify the cell-surface binding property (Fig. 4).

Based on the sequestering effect of EGTA after a prolonged period, we divided the cellular Ca^{2+}-uptake into the EGTA-releasable and the EGTA-nonreleasable pools (Figs. 2 and 3). The EGTA-releasable pool comprises the Ca^{2+} in each cellular compartment as a free ion and as low-affinity binding, to molecules. The EGTA-nonreleasable pool represents the size of high-affinity Ca^{2+} binding to molecules in each compartment. The schematic representation of Fig. 10 summarizes the possible origins of these two pools from the cellular compartments. At different $[Ca^{2+}]_o$ levels, these compartments may contribute differently to the EGTA-releasable and the EGTA-nonreleasable pool size estimated in this study. Based on the previous studies by Brass et al. [8,15], three Ca^{2+}-storage compartments, i.e., cytosol, dense tubular system and mitochondria, may contribute the

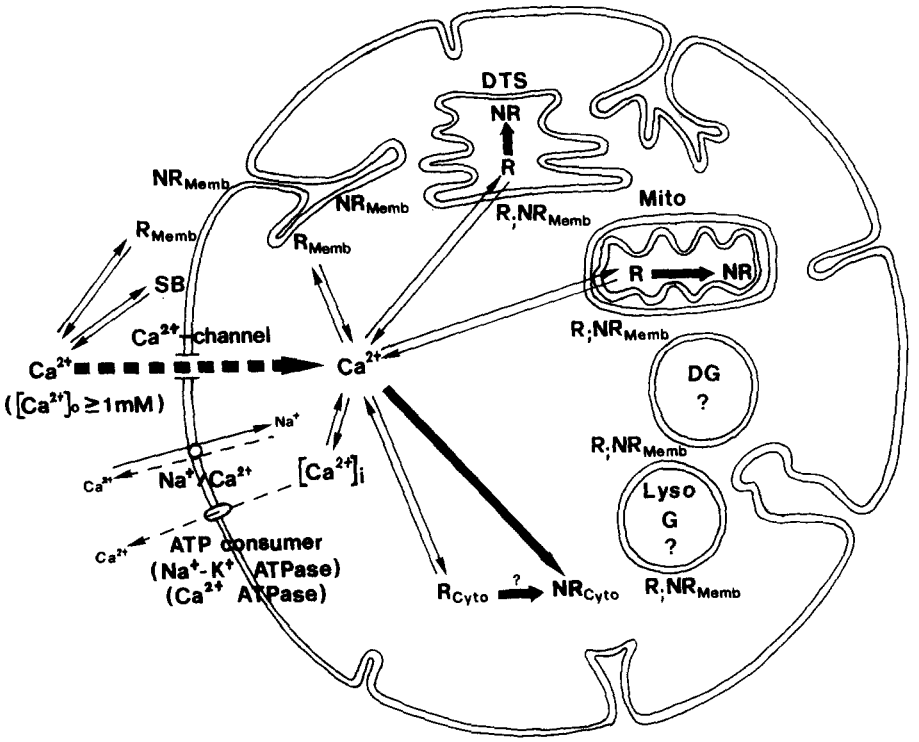

Fig. 10. Schematic representation of the possible contribution of the human platelet Ca^{2+}-storage compartments to the Ca^{2+} pools estimated in this study. During the incubation of platelets in various $[Ca^{2+}]_o$, the platelet surface binds to Ca^{2+} as the surface-bound pool (SB) which represents only the bound Ca^{2+} readily releasable by a transient EGTA chelation. Platelets also sequester Ca^{2+} from $[Ca^{2+}]_o$ into the cytosol through the Ca^{2+}-specific channel (Ca^{2+} channel), as indicated by the large broken arrow. In plasma membrane, the energy-dependent process (ATP consumer) which may be Na^+/K^+-ATPase and Ca^{2+}-ATPase, and the Na^+/Ca^{2+} exchanger (Na^+/Ca^{2+}) are responsible for Ca^{2+} efflux, represented by the narrow broken arrows. The cell is able to maintain a low $[Ca^{2+}]_i$ level by sequestering Ca^{2+} into the EGTA-releasable (R) and EGTA-nonreleasable (NR) pools. Several compartments may contribute to these two pools (R and NR). These compartments are cytosolic molecules (Cyto); dense tubular system (DTS); mitochondria (Mito); and membrane system (R_{Memb}; NR_{Memb}) which includes plasma membrane and cytoplasmic surface of organelle membrane. At different $[Ca^{2+}]_o$, these compartments may contribute different amounts to these two pools. The saturation of the compartments may also be different at low and high $[Ca^{2+}]_o$. The interior of the dense granule (DG), lysosome (Lyso) and other granules (G) may not be involved in these pools; hence, it is indicated by a question mark (?). The narrow arrows indicate the directions of Ca^{2+} flow into the EGTA-releasable pool. The dark arrows represent the major Ca^{2+} flow into the EGTA-nonreleasable pool.

major portion to these two pools. The plasma membrane and cytoplasmic surface of organelle membranes may also contribute to these two pools, since Thompson et al. [16] have reported that the membrane components in either the plasma membrane or the cytoplasmic surface of the orgaelles can associate and release Ca^{2+}. In addition, the plasma membrane outer leaflet may also contribute a small part of these two pools. Some membrane components may bind with a higher affinity to Ca^{2+}, which is not readily releasable by a transient EGTA chelation, to represent the surface-bound pool. In the experimental set up of this study, the interior of the dense granules may not be involved in these pools, since the secretable Ca^{2+} does not seem to exchange with external Ca^{2+} after a short incubation [17,18].

At different $[Ca^{2+}]_o$ levels, these two pools immediately accumulate Ca^{2+} in the first minute (Figs. 2 and 3). The EGTA-releasable pool size then increases at a rate independent of $[Ca^{2+}]_o$, while the rate of increase of the EGTA-nonreleasable pool shows first-order kinetics. In addition, the size ratio of the EGTA-releasable pool to the EGTA-nonreleasable pool appears to be a constant of 3/7 (Table I). These data imply that: (1) the Ca^{2+} release of the cellular compartments is a concentration-dependent process; and (2) the EGTA-nonreleasable pool plays a major role in maintaining a low $[Ca^{2+}]_i$ level. Mitochondria, which is rich in phosphate ions to form calcium phosphates, may contribute the EGTA-nonreleasable pool to a large extent. At low and high $[Ca^{2+}]_o$, the EGTA-releasable and the EGTA-nonreleasable pools may originate differently from each compartment. Therefore, the saturation of each compartment may be in sequence according to the ability of each compartment to store Ca^{2+}. The dense tubular system may become saturated at low $[Ca^{2+}]_o$ levels, while mitochondria may follow, especially at high $[Ca^{2+}]_o$. Subsequently, the EGTA-nonreleasable pool in other compartments may become saturated and a burst of $[Ca^{2+}]_i$ may occur. Then, the damage to organelles results in cell lysis. The lysis occurs after the incubation of platelets in 10 mM $[Ca^{2+}]_o$ at 90 min, in which the EGTA-nonreleasable pool has a saturable capacity of 3000 pmol/10^8 cells, while the EGTA-releasable pool size is about 1100 pmol/10^8 cells (Figs. 2, 3 and 7). The latter may represent the maximum safety capacity of this pool.

Platelets incubated in high $[Ca^{2+}]_o$ appear to undergo a series of morphological changes (Figs. 5–7). This may be due to the elevation of $[Ca^{2+}]_i$, since the morphological change results from the sensitivity of cytoskeletal molecules to $[Ca^{2+}]_i$ [21–26]. During incubation of any length of time, if cells exhibit an alteration in either function or morphology, the $[Ca^{2+}]_i$ value may reflect the dissociation constant (K_d) of Ca^{2+} to the protein molecules responsible for the alteration. The study may indicate that the actin polymerization in platelets is sensitive to $[Ca^{2+}]_i$ at about 160 nM $[Ca^{2+}]_i$, because the cells appear to show pseudopods at $[Ca^{2+}]_i$ near 160 nM. This concentration appears in the platelets incubated at 1, 5 and 10 mM $[Ca^{2+}]_o$ for 120, 60 and 30 min, respectively (Figs. 5–7). The correlation may support a previous report that the K_d of Ca^{2+} to actin monomer is in the nanomolar range [28]. In addition, platelets deform into irregular forms at $[Ca^{2+}]_i < 300$ nM. This $[Ca^{2+}]_i$ is found in the platelets incubated at 1 and 5 mM $[Ca^{2+}]_o$ for 150 and 120 min, respectively (Figs. 5 and 6). Hence, this may mean that the K_d of Ca^{2+} for the microtubule depolymerization is also in the nanomolar range.

The surface-bound Ca^{2+} only represents the Ca^{2+} readily releasable by a transient EGTA chelation (Fig. 4). At $[Ca^{2+}]_o = 1$ mM, the surface capacity is lower than the total cellular uptake. However, at high $[Ca^{2+}]_o$, the surface-bound Ca^{2+} is more than the total uptake by severalfold (Table I). This is due to the acceleration of the surface-binding rate during a prolonged incubation period.

The study of cell-surface Ca^{2+}-binding kinetics indicates that the surface-bound level may be responsible for the acceleration of the binding rate (Fig. 4). The initial binding rate is concentration dependent with a V_{max} of 23.8 pmol/10^8 cells per min. When the capacity of surface-bound Ca^{2+} reaches 160 pmol/10^8 cells (i.e., $9.6 \cdot 10^5$ sites/cell), the binding rate rises 7-fold. This capacity is comparable to the total available Ca^{2+}-binding sties on the platelet surface at physiological $[Ca^{2+}]_o$ [20]. This may mean that a saturation of the physiological binding site causing the membrane to expose more Ca^{2+}-binding sites. Hence, the alteration in the surface-binding rate may originate from the change in the plasma-mem-

brane architecture. The platelet surface appears to have this capacity during incubation in 1 mM $[Ca^{2+}]_o$ for 2 h. This means that the change in the surface-binding property may even effect storage of the cell at physiological $[Ca^{2+}]_o$ (Fig. 4). Another alteration occurs when the surface-bound Ca^{2+} reaches the level of $3.6 \cdot 10^7$ Ca^{2+}/cell. The third kind of binding rate appears to be faster than the initial rate by 11-fold (Fig. 4). The impact of a large amount of Ca^{2+} on the cell surface causes bleb formation, which implies another kind of membrane structure change (Figs. 6 and 7). The formation of blebs may be a Ca^{2+}-specific phenomenon, because: (1) EGTA can abolish blebs immediately; (2) Mg^{2+}, Sr^{2+} and Ba^{2+} do not cause bleb formation; and (3) these ions reacted differently to the Ca^{2+} effect on platelet function (Fig. 9 and Table II). Therefore, the capacity of surface-bound Ca^{2+} is one of the factors critical to platelet physiology. In in vivo systems, the plasma may regulate the platelet surface bound Ca^{2+} to an optimum level.

In summary, this study shows how human platelets respond to incubation in high $[Ca^{2+}]_o$. The continuous increase of Ca^{2+}-pool sizes may explain the gradual morphology changes including pseudopod protrusion, irregular shape deformation, Ca^{2+}-specific surface-bleb formation and cell lysis.

Acknowledgments

This research was supported by a grant from the National Science Council of the Republic of China. We appreciate Drs. Chia-Wei Li, Wen-Guey Wu and Kuan-Rong Lee for their valuable comments on this manuscript. Thanks also to Mr. Young-Ji Shiao and Mr. Jehn-Yuu Lee for their help with the work. This work is a partial fulfillment of Mr. W.J. Tsai's doctoral dissertation.

References

1 Gerrard, J.M., Peterson, D.A. and White, J.G. (1981) in Platelets in Biology and Pathology (Gorrdon, J.L., ed.), Vol. 2, pp. 407–436, Elsevier/North-Holland Biochemical Press, Amsterdam.
2 Luscher, E.F., Massini, P. and Kaser-Glanzmann, R. (1980) in Platelet: Cellular Response Mechanisms and Their Biological Significance (Rotman, A., Meyer, F.A., Gitler, C. and Silberberg, A., eds.), pp. 67–77, John Wiley and Sons, Chichester.
3 Murer, E.H. (1985) Semin. Hematol. 22, 313–323.
4 Barritt, G.J., Parker, J.G. and Wadsworth, J.C. (1981) J. Physiol. 312, 29–55.
5 Rink, T.J., Smith, S.W. and Tsien, R.Y. (1982) FEBS Lett. 148, 21–26.
6 Fisher, G.J., Bakshian, S. and Baldassare, J.J. (1985) Biochem. Biophys. Res. Commun. 129, 958–964.
7 Sage, S.O. and Rink, T.J. (1986) Biochem. Biophys. Res. Commun. 136, 1124–1129.
8 Brass, L.F. (1984) J. Biol. Chem. 259, 12563–12570.
9 Brass, L.F. (1985) J. Biol. Chem. 260, 2231–2236.
10 Powling, M.J. and Hardisty, R.M. (1985) Blood 66, 731–734.
11 Brass, L.F. (1984) J. Biol. Chem. 259, 12571–12575.
12 Rengasamy, A., Soura, S. and Feinberg, H. (1987) Thromb. Haemost. 57, 337–340.
13 Adunyah, S.E. and Dean, W.L. (1986) J. Biol. Chem. 261, 3122–3127.
14 Berridge, M.J. and Irvin, R.F. (1984) Nature 312, 315.
15 Brass, L.F. and Joseph, S.K. (1985) J. Biol. Chem. 260, 15172–15179.
16 Thompson, N.T. and Scrutton, M.C. (1985) Eur. J. Biochem. 147, 421–42.
17 Murer, E.H. (1969) Science 166, 623.
18 Massini, P. and Luscher, E.F. (1976) Biochim. Biophys. Acta 436, 652–663.
19 Seelig, J. and Macdonald, P.M. (1987) Acc. Chem. Res. 20, 221–228.
20 Brass, L.F. and Shattil, S.T. (1982) J. Biol. Chem. 257, 14000–14005.
21 Carroll, R.C., Butler, R.G., Morris, P.A. and Gerrard, J.M. (1982) Cell 30, 385–393.
22 Chadwick Cox, A., Carroll, R.C., White, J.G. and Rao, G.H.R. (1984) J. Cell Biol. 98, 8–15.
23 Fox, J.E.B. and Phillips, D.R. (1983) Semin. Hematol. 20, 243–260.
24 Fox, J.E.B., Boyles, J.K., Reynolds, C.C. and Phillips, D.R. (1984) J. Cell Biol. 98, 1985–1991.
25 Jennings, L.K., Fox, J.E.B., Edwards, H.H. and Phillips, D.R. (1981) J. Biol. Chem. 256, 6927–6932.
26 Steiner, M. and Ikeda, Y. (1979) J. Clin. Invest. 63, 443–448.
27 Gershman, L.C., Selden, L.A. and Estes, J.E. (1986) Biochem. Biophys. Res. Commun. 135, 607–614.
28 Oosawa, F., Asakura, S., Asai, H., Kasai, M., Kobayashi, S., Mihashi, K., Ooi, T., Taniguchi, M. and Nakano, E. (1964) in Biochemistry of Muscle Contraction (Gergely, J., ed.), pp. 158–172, Academic Press, New York.
29 Murer, E.M. (1972) Biochim. Biophys. Acta 261, 435–443.
30 Wang, C.T., Tsai, W.J., Shiao, Y.J., Chen, J.C. and Yang, C.C. (1985) Thrombos. Haemost. 54, 187.
31 Wang, C.T., Tsai, W.J., Chen, J.C., Shiao, Y.J. and Lee, J.Y. (1987) Thrombos. Haemost. 58, 197.
32 Wang, C.-T., Shiao, Y.J., Chen, J.-C., Tsai, W.-J. and Yang, C.-C. (1986) Biochim. Biophys. Acta 856, 244–258.
33 Tsien, R.Y., Pozzan, T. and Rink, T.J. (1982) J. Cell. Biol. 94, 325–334.
34 Bergmeyer, H.U. and Bernt, E. (1974) in Methods of Enzymatic Analysis (Bergmeyer, H.U., ed.), pp. 574–579, Academic Press, New York.
35 Drummond, A.H. and Gordon, J.L. (1974) Thromb. Diath. Haemorrh. 31, 366.